scientific reports

Check for updates

OPEN

Gel permeation chromatography process for highly oriented $Cs_3Cu_2I_5$ nanocrystal film

Yu-Hong Cheng[1], Rikuo Suzuki[1], Narumi Shinotsuka[1], Hinako Ebe[1], Naoaki Oshita[2], Ryohei Yamakado[1], Takayuki Chiba[1]✉, Akito Masuhara[2] & Junji Kido[1]✉

The emergence of green materials has attracted considerable attention in the field of optoelectronics. Copper-based lead-free metal halide (with a near-unity quantum yield) obtained from $Cs_3Cu_2I_5$ nanocrystals (NCs) can exhibit blue emission with a wavelength of 440 nm and provide outstanding stability for various applications. However, in practical applications, colloidal dispersion purity and film quality are inadequate toward a high-performance device. In this study, antisolvent-free gel permeation chromatography is used to purify $Cs_3Cu_2I_5$ NCs. The purified $Cs_3Cu_2I_5$ NCs exhibit a high photoluminescent quantum yield and provide a highly oriented single-crystal film. Density functional theory calculation results indicate that the iodide-rich surface in the NCs makes them highly stable. In addition, it has been demonstrated for the first time that the mixture of polymethyl methacrylate (PMMA) and $Cs_3Cu_2I_5$ NCs has waterproofing capabilities. The composite film consisting of $Cs_3Cu_2I_5$ NCs and PMMA can survive in water for several days. This result opens up more possibilities for the application of these green material.

Cesium lead halide perovskite nanocrystals (NCs) such as $CsPbX_3$ (X = Cl, Br, I) have received tremendous attention for their use as optoelectronic materials in devices such as solar cells[1], light-emitting diodes (LEDs)[2], photodetectors[3,4], and lasers[5] owing to their outstanding optical properties: wide light absorption, high photoluminescence quantum yield (PLQY), and narrow emission spectra with tunable emission peaks. In spite of these advantages, the toxicity of lead and the poor stability at the B site of cesium lead halide perovskite NCs have prevented them from being commercialized[6–8]. In recent years, lead-free perovskite-related NCs containing low-toxicity metals such as tin[9,10], bismuth[11], and antimony[12] have attracted attention as promising light-emitting materials for use in LEDs[13]. However, some challenges still need to be overcome with regard to the use of low-toxicity metals in NCs. For instance, Sn^2 is usually very unstable because of its easy oxidization to tetravalent Sn^{4+} in atmospheric air. In addition, Bi^{3+}-based lead-free NCs exhibit a low PLQY owing to their fast trapping state[14].

More recently, the use of copper(I)-based lead-free metal halide structure as green materials has been demonstrated in the field of optoelectronics[15–28]. The photoluminescence (PL) spectra of lead-free $Cs_3Cu_2I_5$ exhibited a deep blue emission with a broad full width at half maximum (FWHM) and a large Stokes shift, which is attributed to the strong self-trapped emission effect[29]. In particular, lead-free $Cs_3Cu_2I_5$ NCs have the potential to provide strong electron–phonon coupling and a large exciton binding energy, which improve the PL intensity[15]. These NCs can be synthesized via a hot-injection method under high-temperature reaction conditions[30–32], or a ligand-assisted reprecipitation method under room-temperature reaction conditions[16]. However, these NCs require a purification process involving antisolvent reprecipitation, which commonly causes optical quenching and aggregation of NCs. Therefore, an antisolvent-free purification process is urgently needed to realize the application of these NCs in optoelectronic devices. In this context, we previously developed a gel permeation chromatography (GPC) process to remove impurities using only toluene as the nonpolar agent via only one purification cycle[33]. This antisolvent-free purification process has been investigated in the context of core–shell NCs, size selection[34,35], and ligand-exchange[36,37], but has rarely been mentioned in the context of cesium lead halides[38,39].

In this work, we demonstrated the use of antisolvent-free GPC for purifying lead-free $Cs_3Cu_2I_5$ NCs. The purification process completely eliminated impurities in the NCs without causing optical quenching or aggregation. The X-ray diffraction (XRD) patterns of the GPC-purified $Cs_3Cu_2I_5$ NC film exhibited a highly crystalline orientation similar to that of its single-crystal phase. Density functional theory (DFT) calculation results showed that the surface energy of $Cs_3Cu_2I_5$ was the lowest at (020) owing to the high phase stability in the film. The GPC

[1]Graduate School of Organic Materials Science, Yamagata University, 4-3-16 Jonan, Yonezawa, Yamagata 992-8510, Japan. [2]Graduate School of Science and Engineering, Yamagata University, 4-3-16 Jonan, Yonezawa, Yamagata 992-8510, Japan. ✉email: T-chiba@yz.yamagata-u.ac.jp; kid@yz.yamagata-u.ac.jp

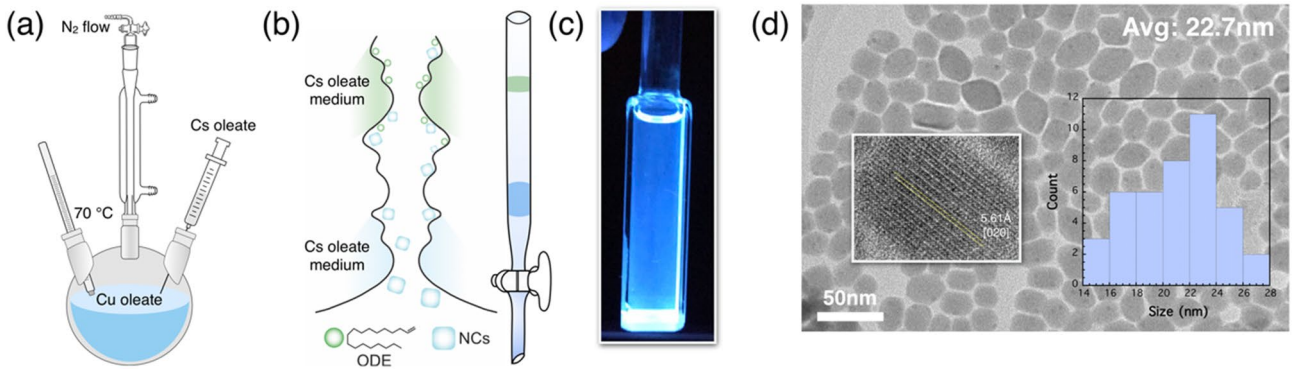

Figure 1. (**a**) Schematic of hot-injection process, (**b**) schematic of purification process, (**c**) image of GPC-purified colloid, and (**d**) TEM image of NCs after GPC purification with *d*-spacing and histogram of particle size.

purified $Cs_3Cu_2I_5$ NCs could be easily spin coated onto the substrate and showed a high PLQY of 79.7% with a peak wavelength of 443 nm and an FWHM of 74.3 nm. In addition, we blended GPC-purified $Cs_3Cu_2I_5$ NCs with polymethyl methacrylate (PMMA) to improve the environmental stability properties of the NCs, such as water and thermal resistance. The PMMA-encapsulated NC-based free-standing film could be used for down-conversion filtering applications. We believe that the antisolvent-free GPC purification process can accelerate the development of lead-free NCs.

Results and discussions

Lead-free $Cs_3Cu_2I_5$ NCs were synthesized via a previously reported hot-injection method with some modifications using cesium iodide (CsI) and copper iodide (CuI) as precursors[32]. We found that the synthesis conditions—ligand concentration and reaction temperature—were optimal for obtaining high-quality $Cs_3Cu_2I_5$ NCs. CuI oleate was prepared by mixing CuI (6 mmol), oleic acid (OA, 6 mL), and oleylamine (OAM, 6 mL) with octadecene (ODE, 100 mL) in a three-neck flask under vacuum at 100 °C. Subsequently, Cs oleate was quickly injected into the CuI oleate solution at 70 °C (Fig. 1a). After 10 s, the reaction mixture was rapidly cooled in an ice bath. The as-synthesized $Cs_3Cu_2I_5$ NCs were isolated via centrifugation at 10,000 rpm for 10 min, and then, the collected $Cs_3Cu_2I_5$ NCs were redispersed in toluene, which was used as a nonpolar solvent. $Cs_3Cu_2I_5$ NCs are very sensitive to polar antisolvents during the reprecipitation process. For instance, when ethyl acetate was used as an antisolvent in the reprecipitation of the NC colloid to remove impurities, the reprecipitated $Cs_3Cu_2I_5$ NCs showed unfavorable crystal growth and a random crystal shape (Figure S1, supplementary information).

Thus, we developed a GPC purification process for $Cs_3Cu_2I_5$ NCs to remove impurities and form a high-quality film. The major benefit of GPC purification is that only toluene is used as a developing solvent in this process, which can produce stable $Cs_3Cu_2I_5$ NCs. The packing medium—polystyrene beads—is a porous and spherical ball, which enables the removal of small molecular hydrocarbon impurities such as ODE or unbound ligands, as shown in Fig. 1b. The $Cs_3Cu_2I_5$ NC toluene colloid (3 mL) was injected into a polystyrene bead-packed column tube (see the Experimental section for details). Purified $Cs_3Cu_2I_5$ NCs (1 mL) were obtained at a concentration of 10 mg mL^{-1} (Fig. 1c). The $Cs_3Cu_2I_5$ NCs had high colloidal stability, considering that the NC solution remained without causing precipitate at least a month. The quantified zeta potential both before and after GPC purification had positive valves: 18.2 and 15.6 mV, respectively. The formation of egg-like $Cs_3Cu_2I_5$ NCs was confirmed by transmission electron microscopy (TEM) and histograms, as shown in Fig. 1d and Figure S2. The average sizes of the NCs before and after GPC purification were 20.7 and 22.7 nm, respectively. The GPC-purified NCs had an interplanar distance of 5.61 Å, which corresponded to the (020) crystal phase.

^{1}H-NMR analysis was performed to determine residual impurities, as shown in Fig. 2a and Figure S3. The $Cs_3Cu_2I_5$ NCs without GPC purification clearly showed alkene resonance related to the ODE at 5.7 to 5.9 ppm, which indicated that the purification was not completed; the OA and OAM related to the range at 5.2 to 5.4 ppm. We started the collection of samples when the $Cs_3Cu_2I_5$ NCs was reached the exit of column. The position of $Cs_3Cu_2I_5$ NCs was checked by UV lamp. In the first fraction, no resonances such as OA and OAM ligands, ODE were observed. Then, the NMR resonance of only surface ligands from $Cs_3Cu_2I_5$ NCs without impurities peaks was observed for the second fraction. Finally, the third fraction showed both of surface ligands and impurities indicating the trapped ODE came together with resident $Cs_3Cu_2I_5$ NCs. The surface ligand composition of the $Cs_3Cu_2I_5$ NC film was confirmed by Fourier transform infrared spectroscopy (FTIR). The FTIR resonance showed the absent of OAM on $Cs_3Cu_2I_5$ NCs surface showed in Fig. 2b. A study pointed out that the OA might tend to absorb onto the NCs, whereas the OAM was likely to desorb and leave the surface[40]. OAM is the primary capping ligand for lead based perovskite and the help of forming soluble molecular species of PbX_2[41]. Therefore, OAM plays a role to form a soluble species of CuI during the Cu-oleate preparation. In addition, X-ray photoelectron spectroscopy (XPS) was used to elucidate the chemical composition of the $Cs_3Cu_2I_5$ NCs (Fig. 2c and Figure S4). The estimated average atomic percentages of Cs, Cu, and I were 26.99%, 17.53%, and 55.47%, respectively, indicating a slightly halide-rich chemical composition. After the GPC process, the chemical composition of the purified NCs remained the same as that before the GPC process (Table S1, supplementary information).

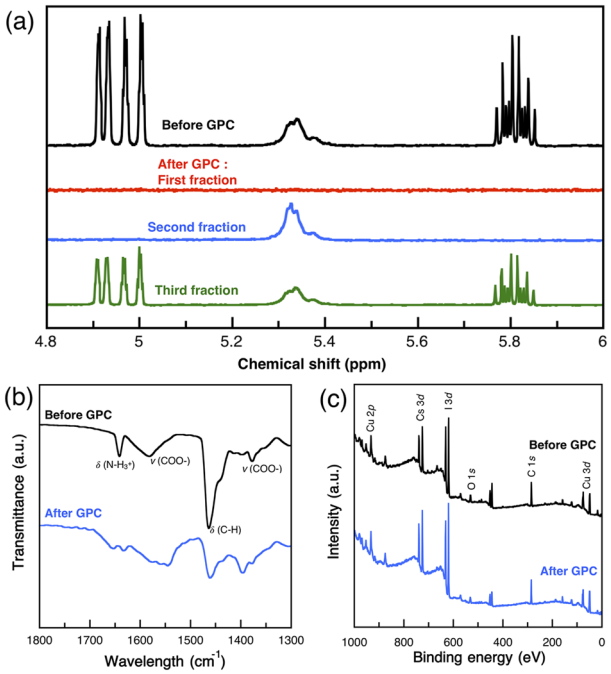

Figure 2. The surface analysis of (**a**) ^{1}H NMR spectra of NCs collected from different fraction of GPC in chloroform-d1, (**b**) FTIR spectra, and (**c**) XPS spectra before and after GPC purification.

$Cs_3Cu_2I_5$ single crystals were prepared from a saturated CsI and CuI precursor solution in dimethyl sulfoxide (DMSO), and then, single-crystal XRD (SXRD) analysis was performed. The obtained crystal data (Pnma, $a = 10.1824(8)$ Å, $b = 11.6655(11)$ Å, and $c = 14.3687(12)$ Å) are consistent with those in previous reports (Table S2)[15,42]. On the other hand, the thin-film XRD analysis of the GPC-purified $Cs_3Cu_2I_5$ NC film showed a simple crystal pattern with peaks at (020), (040), and (060) (Fig. 3a and Table S3). This diffraction pattern matched the calculated diffraction pattern obtained from the single-crystal structure determination. Interestingly, the spin-coated $Cs_3Cu_2I_5$ NC film exhibited a highly oriented single-crystal arrangement in which the *b*-axis was vertical to the substrate, whereas the drop-coated film was randomly arranged. Drop casting was prepared by dropping NCs colloid onto 80℃ Si substrates. Therefore, the XRD peaks of drop coated NCs film were different from the spin coated film due to the random arrangement of $Cs_3Cu_2I_5$ NCs. DFT calculation results showed that the surface energy of the (020) phase (0.117 eV Å^{-2}) was lower than that of the (040) phase (0.145 eV Å^{-2}), indicating that it was easier for the (020) phase than for the (040) phase to form on the surface (Fig. 3b and Figure S5)[40]. In the crystal model, (020) showed an iodide-rich surface, which was consistent with the XPS results.

Furthermore, the SEM image showed a close-packed thin film, which had egg-like shapes that tended to lie flat on the substrate (Fig. 3c). This unique shape is also considered as the factor of promoting the orientated film. Here, we have drop coated NCs colloid onto substrate at different temperatures, there is no obvious difference in the XRD pattern [Figure S6(a)]. On the other hand, the spin coated film had an extra centrifugal force which distinguished the difference in the diffraction pattern. A lower speed coated film showed a similar pattern with drop coated film. As increasing the spin speed, the XRD pattern tend to orientate at (020) and (040) phase [Figure S6(b)]. Therefore, we concluded that the promotion of the orientated film is attributed to the high surface energies, the egg-like shape, and centrifugal force by spin coating process.

The UV–vis absorption and PL spectra of the GPC-purified $Cs_3Cu_2I_5$ NC films are shown in Fig. 3d. The optical band edge of the $Cs_3Cu_2I_5$ NC film was at 316 nm, which corresponded to a bandgap of 3.92 eV. The PL spectra of the $Cs_3Cu_2I_5$ NC film exhibited blue emission at 443 nm with an FWHM of 74.3 nm. The PLQY and PL decay time of the $Cs_3Cu_2I_5$ NCs were 79.3% and 1.284 μs in the film and nearly 100% and 1.236 μs in the colloidal solution, respectively (Figure S7). It is worth mentioning that the PLQY and PL decay time of the colloid before and after GPC purification showed no obvious changes owing to the suppression of optical quenching. Moreover, we dried the colloid using a vacuum pump and redispersed it back into toluene. We found that the PLQY reduced by only approximately 2% without any change in the emission wavelength, which is unlikely to happen in conventional lead halide perovskite NCs (Figure S8). The excellent redispersibility indicates less intense aggregation, compared with a lead-based perovskite, owing to their iodide-rich surface and low surface energy. Therefore, for the first time, we succeeded in investigating the GPC purification of $Cs_3Cu_2I_5$ NCs and their optical properties in the solid film state. The detailed optical properties of the $Cs_3Cu_2I_5$ NCs are listed in Table S4.

The improvement of environmental stability properties such as thermal stability, photostability, and water resistance is a key requirement for various optoelectronic applications. However, $Cs_3Cu_2I_5$ NC films exhibit poor water resistance. We demonstrated for the first time that by blending $Cs_3Cu_2I_5$ NCs with a PMMA polymer composite, a free-standing film could be obtained without a substrate and this film could be used for down-conversion

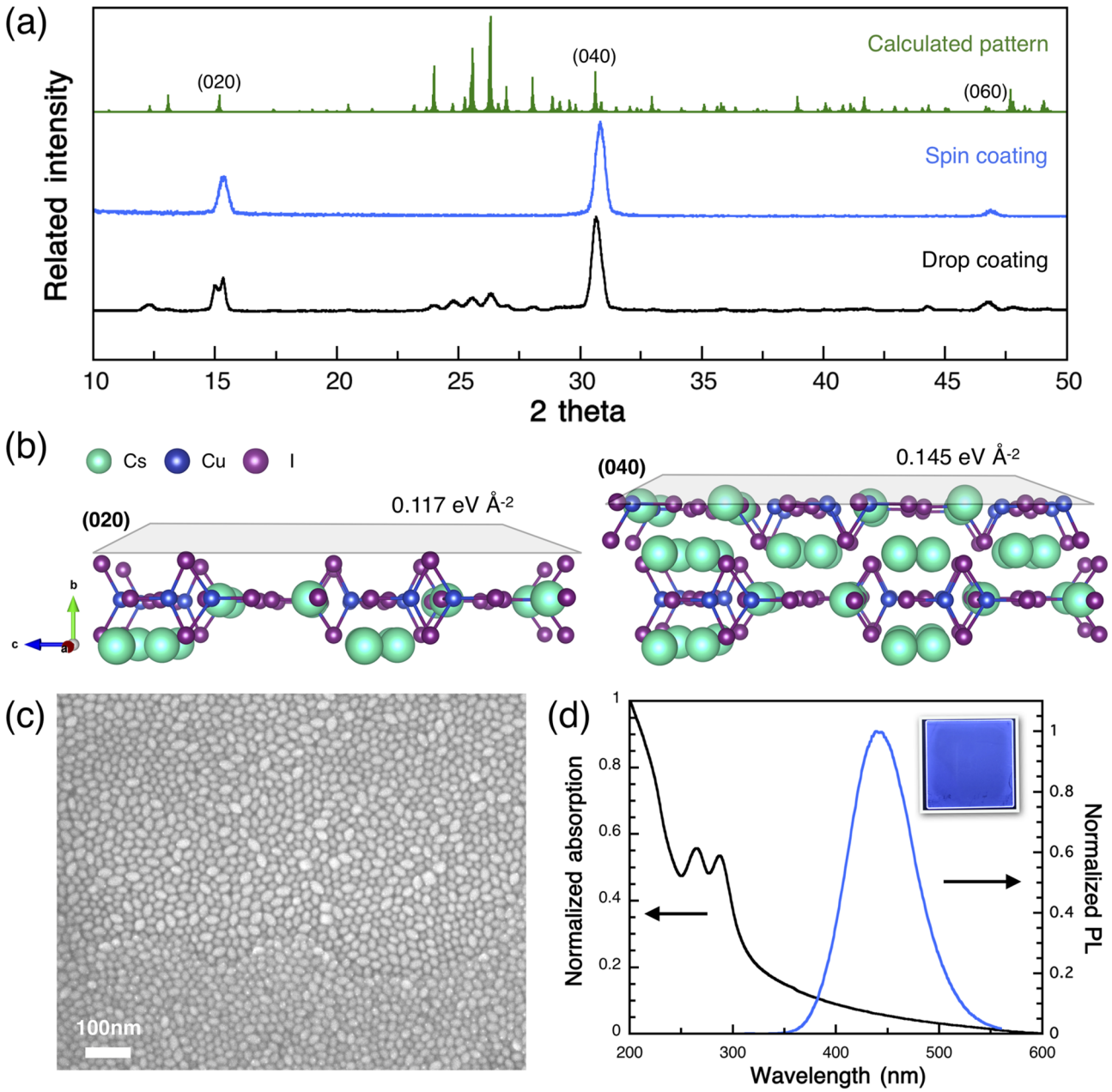

Figure 3. The structure and optical properties of the thin film. (**a**) XRD spectra of spin-coated and drop-coated films, (**b**) crystal structure with different surface directions, (**c**) SEM image of $Cs_3Cu_2I_5$ NC neat film, and (**d**) UV–vis and PL spectra.

filtering applications. The use of chemically stable polymers (PMMA and polystyrene) creates a framework for embedding conventional lead halide perovskite NCs; therefore, the film has improved stability against heat, light, and water owing to the hydrophobic protective property of polymers[43–45]. To prepare the free-standing $Cs_3Cu_2I_5$ NCs blended with the PMMA film, a purified $Cs_3Cu_2I_5$ NC colloidal solution (10 mg mL^{-1} in toluene) was mixed with a PMMA solution (25 wt% in chloroform) in a 1:3 volume ratio, and then, the mixture was kneaded for 2 min. After spin coating the blended film, compression treatment was carried out to produce flat films (Fig. 4a). The PL spectra of the blended film exhibited an emission wavelength of 443 nm with an FWHM of 74.9 nm and was identical to the PL spectra of the $Cs_3Cu_2I_5$ NC neat film (Fig. 4b). The thermal stability of the blended film was tested in a temperature cycle between 25 and 100 °C, as shown in Fig. 4c. The PL intensity decreased as the temperature increased owing to the thermal quenching effect[41]. As the temperature returned to room temperature, the PL intensity also recovered to its initial value, indicating that there was no thermal degradation of the blended film. The blended film exhibited excellent water resistance and maintained the PL intensity even after 10 days at room temperature, as shown in Fig. 4d.

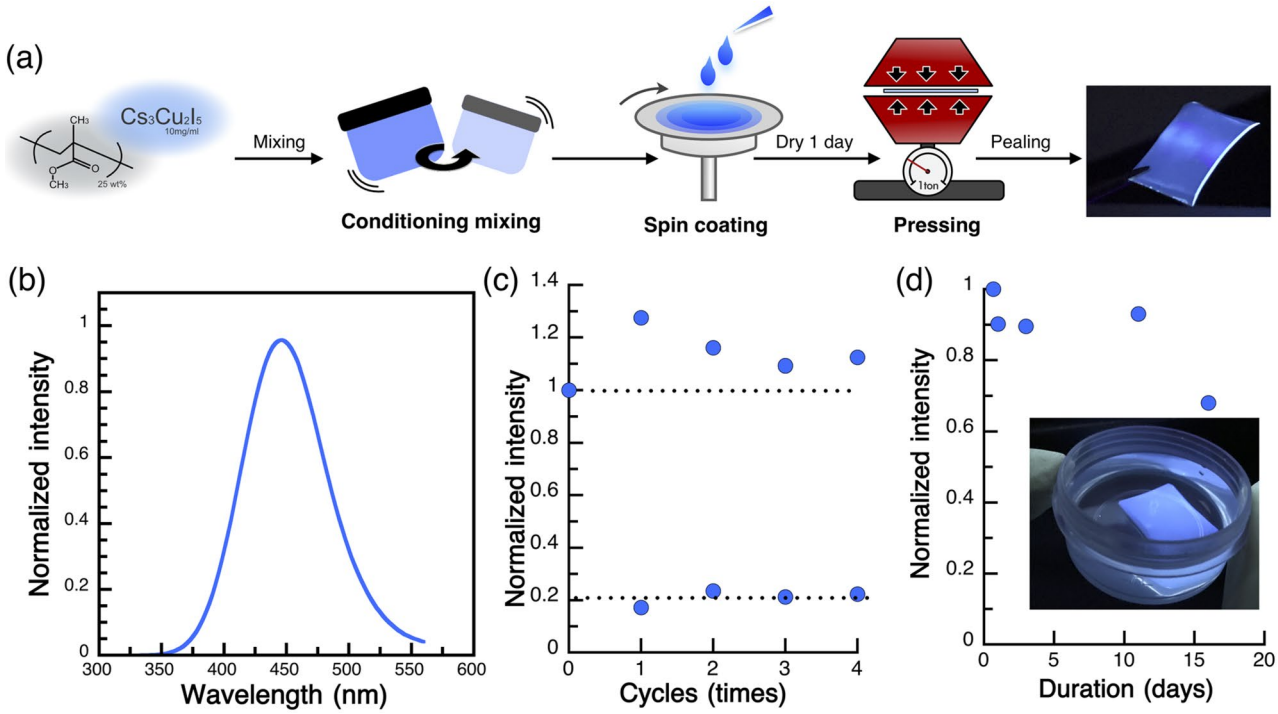

Figure 4. Polymer composite process and its properties. (**a**) Schematic of PMMA-blended NCs, (**b**) PL spectra of PMMA-blended NC film, (**c**) heating/cooling cycling PL measurements, and (**d**) water resistance test showing PL intensity with respect to days.

Conclusion

In this study, polar-solvent-sensitive lead-free $Cs_3Cu_2I_5$ NCs were obtained by GPC purification. The purified $Cs_3Cu_2I_5$ NCs, which did not contain impurities, could form a pin-hole-free thin film. A polystyrene bead-packed column could provide a solution to other lead-free perovskites-related materials that might struggle with the purification process. The $Cs_3Cu_2I_5$ NC film also showed a highly oriented crystal pattern, which was similar to its SXRD pattern, because of its iodide-rich surface and low surface energy. We also found that the oriented feature was further promoted by the unique egg-like sharp after spin coating. Finally, for the first time, we attempted to blend $Cs_3Cu_2I_5$ NCs with PMMA to produce a free-standing film that could survive in water for at least 10 days. The optical properties of the PMMA-mixed $Cs_3Cu_2I_5$ NCs remained the same as those of the unblended NCs, but the ability of the PMMA-mixed $Cs_3Cu_2I_5$ NCs to resist water and humidity was better, which makes them suitable for down-conversion filtering applications.

Materials and methods

Materials. Cesium carbonate (Cs_2CO_3, 99.99%), octadecene (ODE, 90%), oleic acid (OA, 90%), oleylamine (OAM, 80%), were purchased from Sigma-Aldrich. Cesium iodide (CsI, 99.0%) was purchased from Tokyo Chemical Industry. Copper iodide (CuI, 99.0%) was purchased from Kanto Chemical. Poly(methyl methacrylate)(PMMA) pellet were purchased from Fujifilm Wako Pure Chemical. Beads were purchased from BIO-RAD (S-X1). All chemicals were used as received.

Synthesis of $Cs_3Cu_2I_5$ NCs. Pristine $Cs_3Cu_2I_5$ NCs were synthesized via a modified hot-injection method[37]. To prepare Cs oleate, Cs_2CO_3 (273 mg, 0.84 mmol) and OA (0.95 mL, 2.7 mmol) were mixed with ODE (10 mL) in a three-neck flask, and the mixed solution was degassed under a vacuum environment at 120 °C for 1 h. To prepare CuI oleate, OA (6 mL, 17.1 mmol) and OAM (6 mL, 16.4 mmol) were mixed with ODE (100 mL) in a three-neck flask and degassed under vacuum at 120 °C for 1 h. After degassing, the flask was circulated with N_2 flow. Then, CuI (1.1143 g, 6 mmol) was added to the flask at 100 °C until the entire CuI was dissolved. The flask was further cooled to 70 °C, and Cs oleate (8 mL) was quickly injected into it. After 10 s, the reaction was rapidly cooled in an ice bath. The products were isolated by air and centrifuged at 10,000 rpm for 10 min. The precipitates were then redispersed in toluene and recentrifuged at 10,000 rpm for 10 min to collect the supernatant. Finally, the colloid was filtered using a 0.22 μm PTFE filter.

Synthesis of $Cs_3Cu_2I_5$ single crystal. A $Cs_3Cu_2I_5$ solution was prepared using DMSO under ambient conditions. DMSO was slowly added under vigorous stirring until its saturation state, where the concentration was around 0.75 M, and then, the solution was filtered using 0.22 μm PTFE syringe filters. The filtered solution was filled in a vial and covered with a paraffin film with a small hole. The vial was placed inside a bigger bottle

filled with methanol below the vial, and then, the bottle was covered with a paraffin film. The bottle was then placed at room temperature. After 3 days, a single crystal was obtained.

GPC purification process. Beads were allowed to swell overnight in a sample bottle. Then, the swollen beads were packed into a column with a height of approximately 17 cm and a diameter of 10 mm. Dehydrated toluene was made to continuously flow through the column until no free polystyrene was present in the eluent (tested by UV–vis spectroscopy). The $Cs_3Cu_2I_5$ NC colloid (3 mL, obtained as described above) was mildly placed on the top of the column. Approximately 1 ml with concentration of 10 mg mL^{-1} purified dispersion can be obtained. Besides, samples collected at different elution times are used for characterization. All the steps were carried out inside a N_2-filled glove box.

Fabrication of blended NC PMMA film. A PMMA/chloroform solution (25 wt%) was prepared as follows. PMMA pellets (10 g) were dissolved in chloroform (20.1 mL) at 55 °C. The NC and PMMA/chloroform solutions (10 mg mL^{-1}) were mixed in a 1:3 volume ratio; the mixture was then kneaded and defoamed. To fabricate the NC PMMA film, the NC PMMA mixed solution (1 mL) was spin coated onto a glass substrate at 50 rpm for 1000 s. Finally, the film was left in a darkroom for 1 day, and it was compressed under a weight of 1 ton for 1 min to form a flat surface.

Characterization. Scanning electron microscope (SEM) imaging was took using JEOL JSM-6700F system operated at 15 kV, the samples were prepared by using ITO substrate. Transmission electron microscopy (TEM) analysis was performed using a JEOL JEM-2100F microscope operating at 200 kV. The NMR spectra were obtained using a JEOL 400 spectrometer operated at a ^1H frequency of 500 MHz. FTIR was performed using a JASCO FT/IR-4700. The chemical compositions were determined by XPS (Thermo Fisher Scientific Theta probe). The single-crystal XRD data were collected using a Rigaku RAPID-II diffractometer with graphite monochromated Mo Kα radiation (λ = 0.71075 Å), while the out-of-plane XRD spectra were measured by a Rigaku SmartLab diffractometer using Cu-Ka raditation as the X-ray source; the sample was coated onto Si substrate. The photoluminescence spectra were measured using a HORIBA FluoroMax-2 luminescence spectrometer with a Xe lamp; PLQY were measured using a Hamamatsu C9920-01 integral sphere system at an exciton intensity of ~ 1 uW cm^{-2} with a Xe lamp, both PL and PLQY were measured by an excitation wavelength of 290 nm. Photoluminescence decay was determined using a Hamamatue C11367 Quantaurus-Tau system with an excitation wavelength of 280 nm. The UV–vis-absorption spectra were measured using a Shimadzu UV-3150 UV–vis-NIR spectrophotometer; all the optical measurements were performed by using quartz substrate. The water resistant was performed by immersed NCs + PMMA film into deionized water kept at room temperature. The zeta potential was performed using MALVERN Nano ZS.

Data availability

Materials and data are available.

Received: 10 August 2021; Accepted: 21 February 2022
Published online: 17 March 2022

References

1. Correa-Baena, J.-P. *et al.* Promises and challenges of perovskite solar cells. *Science* **358**, 739–744 (2017).
2. Liu, X. K. *et al.* Metal halide perovskites for light-emitting diodes. *Nat. Mater.* **20**, 10–21. https://doi.org/10.1038/s41563-020-0784-7 (2021).
3. Zhang, J. *et al.* High-performance transparent ultraviolet photodetectors based on inorganic perovskite CsPbCl3 nanocrystals. *RSC Adv.* **7**, 36722–36727. https://doi.org/10.1039/c7ra06597c (2017).
4. Wang, H. P. *et al.* Low-dimensional metal halide perovskite photodetectors. *Adv. Mater.* **33**, e2003309. https://doi.org/10.1002/adma.202003309 (2021).
5. Dong, H., Zhang, C., Liu, X., Yao, J. & Zhao, Y. S. Materials chemistry and engineering in metal halide perovskite lasers. *Chem. Soc. Rev.* **49**, 951–982. https://doi.org/10.1039/c9cs00598f (2020).
6. Prakasam, V., Tordera, D., Bolink, H. J. & Gelinck, G. Degradation mechanisms in organic lead halide perovskite light-emitting diodes. *Adv. Opt. Mater.* **7**, 1900902. https://doi.org/10.1002/adom.201900902 (2019).
7. Lou, S., Xuan, T. & Wang, J. (INVITED) Stability: A desiderated problem for the lead halide perovskites. *Opt. Mater.* **1**, 100023. https://doi.org/10.1016/j.omx.2019.100023 (2019).
8. Schileo, G. & Grancini, G. Lead or no lead? Availability, toxicity, sustainability and environmental impact of lead-free perovskite solar cells. *J. Mater. Chem. C* **9**, 67–76. https://doi.org/10.1039/d0tc04552g (2021).
9. Hong, W. L. *et al.* Efficient low-temperature solution-processed lead-free perovskite infrared light-emitting diodes. *Adv. Mater.* **28**, 8029–8036. https://doi.org/10.1002/adma.201601024 (2016).
10. Yuan, F. *et al.* Color-pure red light-emitting diodes based on two-dimensional lead-free perovskites. *Sci. Adv.* **6**, eabb0253 (2020).
11. Leng, M. *et al.* All-inorganic bismuth-based perovskite quantum dots with bright blue photoluminescence and excellent stability. *Adv. Funct. Mater.* **28**, 1704446. https://doi.org/10.1002/adfm.201704446 (2018).
12. Ma, Z. *et al.* Electrically-driven violet light-emitting devices based on highly stable lead-free perovskite Cs3Sb2Br 9 quantum dots. *ACS Energy Lett.* **5**, 385–394. https://doi.org/10.1021/acsenergylett.9b02096 (2019).
13. Zhang, F. *et al.* Recent advances and opportunities of lead-free perovskite nanocrystal for optoelectronic application. *Energy Mater. Adv.* **1–38**, 2021. https://doi.org/10.34133/2021/5198145 (2021).
14. Yang, B. *et al.* Lead-free, air-stable all-inorganic cesium bismuth halide perovskite nanocrystals. *Angew. Chem. Int. Ed.* **56**, 12471–12475. https://doi.org/10.1002/anie.201704739 (2017).
15. Jun, T. *et al.* Lead-free highly efficient blue-emitting Cs3 Cu2 I5 with 0D electronic structure. *Adv. Mater.* **30**, e1804547. https://doi.org/10.1002/adma.201804547 (2018).
16. Li, Y. *et al.* Room temperature synthesis of stable, printable Cs3Cu2X5 (X = I, Br/I, Br, Br/Cl, Cl) colloidal nanocrystals with near-unity quantum yield green emitters (X = Cl). *Chem. Mater.* **32**, 5515–5524. https://doi.org/10.1021/acs.chemmater.0c00280 (2020).

17. Guo, Z. *et al.* All-inorganic copper(i)-based ternary metal halides: promising materials toward optoelectronics. *Nanoscale* **12**, 15560–15576. https://doi.org/10.1039/d0nr04220j (2020).
18. Liu, X. *et al.* Vacuum dual-source thermal-deposited lead-free Cs3Cu2I5 films with high photoluminescence quantum yield for deep-blue light-emitting diodes. *ACS Appl. Mater. Interfaces* **12**, 52967–52975. https://doi.org/10.1021/acsami.0c17029 (2020).
19. Wang, L. *et al.* Colloidal synthesis of ternary copper halide nanocrystals for high-efficiency deep-blue light-emitting diodes with a half-lifetime above 100 h. *Nano Lett.* **20**, 3568–3576. https://doi.org/10.1021/acs.nanolett.0c00513 (2020).
20. Zhang, F. *et al.* Strongly emissive lead-free 0D Cs3Cu2I5 perovskites synthesized by a room temperature solvent evaporation crystallization for down-conversion light-emitting devices and fluorescent inks. *Adv. Opt. Mater.* **8**, 1901723. https://doi.org/10.1002/adom.201901723 (2020).
21. Lian, L. *et al.* Efficient and reabsorption-free radioluminescence in Cs3Cu2I5 nanocrystals with self-trapped excitons. *Adv. Sci.* **7**, 2000195. https://doi.org/10.1002/advs.202000195 (2020).
22. Liang, W. Q. *et al.* A solution-processed ternary copper halide thin films for air-stable and deep-ultraviolet-sensitive photodetector. *Nanoscale* **12**, 17213–17221. https://doi.org/10.1039/d0nr03630g (2020).
23. Liang, W. *et al.* Strategy of all-inorganic Cs3Cu2I5/Si-core/shell nanowire heterojunction for stable and ultraviolet-enhanced broadband photodetectors with imaging capability. *ACS Appl. Mater. Interfaces* **12**, 37363–37374. https://doi.org/10.1021/acsami.0c10323 (2020).
24. Zeng, F. *et al.* Opportunity of the lead-free all-inorganic Cs3Cu2I5 perovskite film for memristor and neuromorphic computing applications. *ACS Appl. Mater. Interfaces* **12**, 23094–23101. https://doi.org/10.1021/acsami.0c03106 (2020).
25. Zeng, F. *et al.* Impact of hydroiodic acid on resistive switching performance of lead-free Cs3Cu2I5 perovskite memory. *J. Phys. Chem. Lett.* **12**, 1973–1978. https://doi.org/10.1021/acs.jpclett.0c03763 (2021).
26. Vashishtha, P. *et al.* Cesium copper iodide tailored nanoplates and nanorods for blue, yellow, and white emission. *Chem. Mater.* **31**, 9003–9011. https://doi.org/10.1021/acs.chemmater.9b03250 (2019).
27. Ma, Z. *et al.* High color-rendering index and stable white light-emitting diodes by assembling two broadband emissive self-trapped excitons. *Adv. Mater.* **33**, e2001367. https://doi.org/10.1002/adma.202001367 (2021).
28. Liu, S. *et al.* A controllable and reversible phase transformation between all-inorganic perovskites for white light emitting diodes. *J. Mater. Chem. C* **8**, 8374–8379. https://doi.org/10.1039/d0tc01519a (2020).
29. Lin, R. *et al.* Dual self-trapped exciton emission with ultrahigh photoluminescence quantum yield in CsCu2I3 and Cs3Cu2I5 perovskite single crystals. *J. Phys. Chem. C* **124**, 20469–20476. https://doi.org/10.1021/acs.jpcc.0c07435 (2020).
30. Luo, Z. *et al.* 0D Cs3 Cu2 X5 (X = I, Br, and Cl) nanocrystals: Colloidal syntheses and optical properties. *Small* **16**, e1905226. https://doi.org/10.1002/smll.201905226 (2020).
31. Lian, L. *et al.* Photophysics in Cs3Cu2X5 (X = Cl, Br, or I): Highly Luminescent Self-Trapped Excitons from Local Structure Symmetrization. *Chem. Mater.* **32**, 3462–3468. https://doi.org/10.1021/acs.chemmater.9b05321 (2020).
32. Cheng, P. *et al.* Colloidal synthesis and optical properties of all-inorganic low-dimensional cesium copper halide nanocrystals. *Angew. Chem. Int. Ed.* **58**, 16087–16091. https://doi.org/10.1002/anie.201909129 (2019).
33. Ebe, H., Chiba, T., Ohisa, S. & Kido, J. Gel permeation chromatography purification process for highly efficient perovskite nanocrystal light-emitting devices. *J. Photopolym. Sci. Tec.* **33**, 393–397 (2020).
34. Pitkanen, L. & Striegel, A. M. Size-exclusion chromatography of metal nanoparticles and quantum dots. *Trends Analyt. Chem.* **80**, 311–320. https://doi.org/10.1016/j.trac.2015.06.013 (2016).
35. Liu, J., Enomoto, K., Takeda, K., Inoue, D. & Pu, Y.-J. Simple cubic self-assembly of PbS quantum dots by finely controlled ligand removal through gel permeation chromatography. *Chem. Sci.* **12**, 10354–10361 (2021).
36. Shen, Y. *et al.* Gel permeation chromatography as a multifunctional processor for nanocrystal purification and on-column ligand exchange chemistry. *Chem. Sci.* **7**, 5671–5679. https://doi.org/10.1039/c6sc01301e (2016).
37. Roberge, A., Stein, J. L., Shen, Y., Cossairt, B. M. & Greytak, A. B. Purification and in situ ligand exchange of metal-carboxylate-treated fluorescent InP quantum dots via gel permeation chromatography. *J. Phys. Chem. Lett.* **8**, 4055–4060. https://doi.org/10.1021/acs.jpclett.7b01772 (2017).
38. Dong, Y. *et al.* Precise Control of Quantum Confinement in Cesium Lead Halide Perovskite Quantum Dots via Thermodynamic Equilibrium. *Nano Lett.* **18**, 3716–3722. https://doi.org/10.1021/acs.nanolett.8b00861 (2018).
39. Abiodun, S. L., Pellechia, P. J. & Greytak, A. B. Effective purification of CsPbBr 3 nanocrystals with high quantum yield and high colloidal stability via gel permeation chromatography. *J. Phys. Chem. C* **125**, 3463–3471 (2021).
40. Pan, J. *et al.* Highly efficient perovskite-quantum-dot light-emitting diodes by surface engineering. *Adv. Mater.* **28**, 8718–8725 (2016).
41. Zhang, Y. *et al.* A "tips and tricks" practical guide to the synthesis of metal halide perovskite nanocrystals. *Chem. Mater.* **32**, 5410–5423. https://doi.org/10.1021/acs.chemmater.0c01735 (2020).
42. Hull, S. & Berastegui, P. Crystal structures and ionic conductivities of ternary derivatives of the silver and copper monohalides—II: ordered phases within the (AgX)x–(MX)1–x and (CuX)x–(MX)1–x (M=K, Rb and Cs; X=Cl, Br and I) systems. *J. Solid State Chem.* **177**, 3156–3173. https://doi.org/10.1016/j.jssc.2004.05.004 (2004).
43. Xin, Y., Zhao, H. & Zhang, J. Highly stable and luminescent perovskite-polymer composites from a convenient and universal strategy. *ACS Appl. Mater. Interfaces* **10**, 4971–4980. https://doi.org/10.1021/acsami.7b16442 (2018).
44. Tong, J. *et al.* Direct hot-injection synthesis of lead halide perovskite nanocubes in acrylic monomers for ultrastable and bright nanocrystal-polymer composite films. *ACS Appl. Mater. Interfaces* **11**, 9317–9325. https://doi.org/10.1021/acsami.8b20681 (2019).
45. Tai, C. L. *et al.* Ultrastable, deformable, and stretchable luminescent organic-inorganic perovskite nanocrystal-polymer composites for 3D printing and white light-emitting diodes. *ACS Appl. Mater. Interfaces* **11**, 30176–30184. https://doi.org/10.1021/acsami.9b06248 (2019).

Acknowledgements

The authors acknowledge a "Grant-in Aid for Scientific Research C" (20K05639) from the Japan Society for the Promotion of Science (JSPS) and Extensive Support for Young Promising from the New Energy and Industrial Technology Development Organization (NEDO). The authors also want to acknowledge the support provided by the Adaptable and Seamless Technology Transfer Program through Target-driven R&D (A-STEP) and the Center of Innovation Program from the Japan Science and Technology Agency (JST).

Author contributions

Y.C. and T.C. conceived and designed the experiments. S.N. perform the XPS and TEM measurement. Y.C. performed the UV–vis absorption, PL, PL-decay, IR, and stability test. Y.C. and H.E. performed the GPC process. R.S. performed the simulation calculation. A.M. and N.O. developed and produced the polymer composite film. T.C. assisted with the materials and characterization process. R.Y. assisted with the XRD characterization. J.K. supervised this work. Y.C. and T.C. wrote the manuscript. All the authors have read and commented on the manuscript.

Competing interests
The authors declare no competing interests.

Additional information
Supplementary Information The online version contains supplementary material available at https://doi.org/10.1038/s41598-022-08760-6.

Correspondence and requests for materials should be addressed to T.C. or J.K.

Reprints and permissions information is available at www.nature.com/reprints.

Publisher's note Springer Nature remains neutral with regard to jurisdictional claims in published maps and institutional affiliations.